A Shear Mode Piezoelectric Energy Harvester Based on a Pressurized Water Flow

Dung-An Wang, Nine-Zeng Liu

Graduate Institute of Precision Engineering, National Chung Hsing University, Taichung 40227, Taiwan, ROC

Abstract

A shear mode piezoelectric energy harvester for harnessing energy from pressurized water flow is developed. It converts flow energy into electrical energy by piezoelectric conversion with oscillation of a piezoelectric film. A finite element model is developed in order to estimate the generated voltage of the piezoelectric film subjected to a distributed load. Prototypes of the energy harvester are fabricated and tested. Experimental results show that an open circuit output voltage of 72 mV_{pp} and an instantaneous output power of 0.45 nW are generated when the excitation pressure oscillates with an amplitude of 20.8 kPa and a frequency of about 45 Hz. The solution of the generated voltage based on the finite element model agrees well with the experiments. Based on the finite element model, the effects of the piezoelectric film dimensions, the water pressure and types of piezoelectric films on the output voltage of the harvester can be investigated.

Keywords: Piezoelectric; Shear mode; Energy harvester; Finite element analysis

---

[*] Corresponding author. Tel.:+886-4-22840531; fax:+886-4-22858362

E-mail address: daw@dragon.nchu.edu.tw (D.-A. Wang).

1. Introduction

In order to recover wasted energy, many mesoscale schemes are presented, such as a thermoelectric harvester worn on human wrist that delivered a power of about 0.3 nW [1], and an electromagnetic harvester based on a turbine driven by water pressure drop in throttling valves and turbo expanders in plants that output a power of 150 W [2]. In recent years a considerable effort was focused on use of improved piezoelectric devices in the development of energy harvesters or micropower generators. By scavenging energy from the environment, miniature sensing/actuating devices can be self-powered in order to avoid the replacement of finite power sources. The development of microsystems located in harsh environment further demands for low power consumption and almost no maintenance requirement.

One approach to harvest energy is to convert mechanical energy of ambient vibration into electrical energy by piezoelectric devices. Piezoelectric harvesters have been proposed and investigated by many researchers due to its high energy density, for example, see [3-12]. Different piezoelectric modes were adopted for piezoelectric energy harvesters. Fang et al. [6] developed a 31 mode piezoelectric cantilever for energy harvesting. The piezoelectric layer is fabricated on top of a silicon layer. When used in a bending mode, the laminated piezoelectric layer develops much higher voltage output when flexed than a non-laminated piezoelectric layer. The neutral axis is in the silicon layer instead of in the piezoelectric layer so the piezoelectric layer is strained more when flexed. The power density of their device was estimated as 10843 $\mu W\ cm^{-3}$. Shen et al. [13] designed a 31 mode piezoelectric energy harvester for low frequency (hundreds of hertz) and high acceleration (> 1 g, $g = 9.81\ m \cdot sec^{-2}$) vibration applications. Their device was of a cantilever beam type with the proof mass integrated with the cantilever to avoid the additional difficulty in fabrication, and a power density of 3272 μW cm^{-3} was reported. Marzencki et al. [14] also presented a 31 mode piezoelectric energy harvester of a cantilever beam type. The dimensions of their device are an outcome of an optimization process using finite element models and analytical models. The power density of their device was estimated as 3569 μW cm^{-3} based on the data described by Marzencki et al. [14]. A 33 mode piezoelectric energy harvester was developed by Jeon et al. [15], where the electrodes were patterned into an interdigitated shape on the piezoelectric cantilever. Their 33 mode design generated a voltage 20 times higher than that of a 31 mode design of the same dimension [15]. The higher voltage output can be explained by the fact that the magnitudes of the piezoelectric constant, d_{33}, are generally 2-2.5 times higher than the piezoelectric constant, d_{31}. Using piezoelectric materials for energy harvesting/sensing, the shear type, 15 mode, might provide a larger output as compared to the 31 and 33 modes for certain loading cases [16]. Edery-Azulay and Abramovich [16] found that for cases of low lateral displacements, the 15 mode has a greater output than the 31 mode, and by decreasing the thickness of the 15 mode piezoelectric beam while keeping its volume the same, the efficiency of the 15 mode can become much bigger than that of the 31 mode. Ren et al. [17] presented a 15 mode piezoelectric cantilever beam for energy harvesting. The single crystal of $0.71Pb(Mg_{1/3}Nb_{2/3})O_3 - 0.29PbTiO_3$ was selected as the piezoelectric material of their device due to its ultrahigh d_{15} value, which can reach the high value of 5980 $pm \cdot V^{-1}$. A peak voltage of 91.23 V and a maximum power of 4.16 mW of their device with a d_{15}

value of 3080 $\text{pm} \cdot \text{V}^{-1}$ were reported, and the estimated power density is 24762 $\mu\text{W cm}^{-3}$. Majidi et al. [18] introduced an array of ZnO nanoribbons for energy harvesting bases on the 15 mode piezoelectric coupling. They predicted that the device can produce as much as 100 $\mu\text{W cm}^{-3}$ from elastic deformations induced by sliding friction or mechanical vibration. These investigations provide a proper perspective on the potential of utilizing the 15 mode piezoelectric coupling for energy harvesting.

Energy harvesting through an elastically mounted seismic mass through base excitation has been exploited extensively in an attempt to demonstrate the idea of vibration-to-electric energy conversion [3,19-28]. The energy source for vibration-driven energy harvesters could be the kinetic energy of fluid motion. Several investigations have addressed the feasibility of kinetic energy conversion from fluid motion into mechanical energy of a resonator. Allen and Smits [3] used a piezoelectric membrane placed behind the von Kármán vortex street formed behind a bluff body to harvest energy from fluid motion. They examined the response of the membrane to vortex shedding. The power output of the membrane is not presented. Taylor et al. [29] developed an eel structure of piezoelectric polymer to convert mechanical flow energy to electrical power. The 31 mode of the piezoelectric material was utilized for energy harvesting by their eel device. Tang et al. [30] presented a flutter-mill to generate electricity by extracting energy from fluid flow. Their plate with embedded conductors fluttered between a pair of magnetic panels during fluid flow, and an electric potential difference was generated on the plate. Considering the energy density, it appears that piezoelectric harvesters are capable of producing higher power output than electromagnetic and electrostatic harvesters [31]. The values of the piezoelectric constant, d_{15}, are generally higher than those of d_{31} and d_{33} [32]. A 15 mode piezoelectric device with simple structure design and ease of application may be needed to extract energy from fluid motion.

In this paper, we develop a shear mode (15 mode) energy-harvesting device based on pressurized water flow. The focus is to demonstrate the feasibility of using a shear mode piezoelectric film for energy harvesting from fluid motion. As illustrated in Fig. 1, a flow channel with a flexible diaphragm is connected to a flow source. The pressure in the chamber causes the diaphragm to deflect in the upward direction. As the pressure increases to the maximum, the diaphragm reaches its highest position. When the pressure drops, the diaphragm moves downward. As the pressure decreases to the minimum, the diaphragm reaches its lowest position. Thus, by connecting the energy harvester to an ambient flow source, which is capable of providing the pressure change in the pressure chamber, the oscillating movement of the diaphragm with the piezoelectric film attached to it makes the energy harvesting possible. The focus of this paper is on the investigation of using a shear mode piezoelectric film for energy harvesting from a fluid flow. In order to access the feasibility of the proposed energy harvester, finite element analyses are carried out to estimate the output voltage of the piezoelectric film. Fabrication of the energy harvester with an electroforming process and an assembly technique is described. Experimental setup used to measure water pressure in the flow channel, and the deflection and voltage output of the device is reported. The fabricated device is tested under various loading conditions. The experimental results are compared with the results of the analyses.

2. Design

2.1 Operational principle

Our design of the shear mode piezoelectric energy harvester is based on the vibration induced by pressurized water flow in channels. The variation of the liquid pressure in the channel drives a nickel (Ni) flexible diaphragm and a piezoelectric film into vibration. The vibration energy is converted to electrical energy by the piezoelectric film. A shear mode piezoelectric energy harvester is shown in Fig. 2(a). Fig. 2(b) is an exploded view of the energy harvester. It consists of a flow channel with two glass tubes, a Ni diaphragm embedded in a Ni plate which is bonded to the channel, and a piezoelectric film glued to the Ni plate and a Ni bulge. The Ni bulge, Ni diaphragm and Ni plate are an integral part which is fabricated by an electroforming process. The Ni bulge serves the purpose to translate the up and down movement of the Ni diaphragm to the piezoelectric film.

Fig. 3(a) shows the polarization direction of the shear mode piezoelectric film. Five zones including two poled zones, P, and three non-poled zones, NP, are indicated in the figure. The two poled zones have opposite polarization directions. When the diaphragm moves upward, the piezoelectric film strains transversely and an electric field perpendicular to the polarization directions is established across the thickness direction of the piezoelectric film (see Fig. 3(b)). When the diaphragm moves downward, the electric field in the piezoelectric film reverses its direction (see Fig. 3(c)). In order to impart uniform polarization for the shear mode piezoelectric film, the poling electrodes are arranged on both the top and bottom surfaces of the piezoelectric film. This poling design provides a uniform and efficient polarization of the shear mode piezoelectric film [33].

This harvesting of flow energy via a flow-induced vibration is related to the response of a flexible diaphragm to an internal flow. The flow is bounded by the flexible structure and rigid walls. If the diaphragm has small inertia and is flexible enough to be able to respond rapidly to the fluctuating pressure field set up by the flow, one may expect that the diaphragm may oscillate with a frequency similar to that observed in the flow. When the fluctuating pressure is applied on the surface of the diaphragm, the piezoelectric film stressed transversely. The shear stress causes electrical charge to accumulate on the piezoelectric electrodes, resulting in a voltage in the thickness direction of the shear mode piezoelectric film. For convenience of analysis, a simple model is developed to estimate the voltage generated in the piezoelectric film.

2.2 A model for estimation of the voltage generated in the piezoelectric film

Using Gauss's law, the charge accumulated on the piezoelectric electrodes is given by

$$Q = \oint_S D_z dA \tag{1}$$

where D_z is the electrical displacement in the thickness direction of the piezoelectric film, and dA is a differential area on the electrode surface S. For the piezoelectric film mounted on the diaphragm as shown in Fig. 2(b), we have

$$\begin{bmatrix} D_x \\ D_y \\ D_z \end{bmatrix} = \begin{bmatrix} 0 & 0 & 0 & d_{15} & 0 & 0 \\ d_{31} & d_{33} & d_{31} & 0 & 0 & 0 \\ 0 & 0 & 0 & 0 & 0 & d_{15} \end{bmatrix} \begin{bmatrix} \sigma_{xx} \\ \sigma_{yy} \\ \sigma_{zz} \\ \sigma_{xy} \\ \sigma_{xz} \\ \sigma_{yz} \end{bmatrix} \tag{2}$$

where σ_{xx}, σ_{yy} and σ_{zz} are the normal stresses in the x, y and z direction, respectively, and σ_{xy}, σ_{xz} and σ_{yz} are the shear stresses. A Cartesian coordinate system is indicated in Fig. 2(a). d_{31}, d_{33} and d_{15} are piezoelectric constants. D_x and D_y are the electrical displacements in the width and length direction of the piezoelectric film, respectively. Using Equation (2), D_z can be written as

$$D_z = d_{15}\sigma_{yz} \tag{3}$$

The voltage generated in the piezoelectric film can be expressed as

$$V = \frac{Q}{C} \tag{4}$$

where C is the capacitance of the piezoelectric film.

Due to the geometry and loading of the device, finite element analyses are carried out to obtain the shear stress σ_{yz} in the piezoelectric film. The dimensions of the energy harvester are indicated in Fig. 2(b). The dimensions of the poled zones of the piezoelectric film are also shown in Fig. 2(b). A Cartesian coordinate system is shown in the figure. Due to symmetry, only a quarter model is considered. Fig. 4(a) shows a schematic of a quarter model of the piezoelectric film, the bulge and the flexible diaphragm. As shown in Fig. 4(a), the deflections in the x, y and z directions of the flexible diaphragm at the circumference of the pressure chamber are constrained to represent the fixed boundary conditions. The bottom surface of the piezoelectric film is rigidly connected to the top surface of the bulge. A pressure P is applied at the bottom surface of the diaphragm. The displacement in the x and y direction of the symmetry plane, the $y-z$ and $x-z$ plane, respectively, is constrained to represent the symmetry condition due to the loading conditions and the geometry of the device. Fig. 4(b) shows a mesh for a finite element model. Fig. 4(c) shows a close-up view of the mesh near the center of the diaphragm. The Ni flexible diaphragm has a thickness of 10 μm. The electrode layers with a thickness of 10 μm are attached the top and bottom surfaces of the piezoelectric film of 200 μm. The finite element model has 4319 20-node quadratic elements. A mesh convergence study is performed to obtain accurate solutions of charge accumulation.

The material properties of the piezoelectric film (PZT-5H), the electrodes (silver), the bulge and the diaphragm (Ni) are listed in Table 1. The commercial finite element program ABAQUS [34] is employed to perform the computations. 20-node piezoelectric element C3D20RE is used to model the poled zone of the piezoelectric film. The element type used for the non-poled zone of the piezoelectric film, the electrode, the bulge and the diaphragm is the 20-node element C3D20R.

2.3 Analysis

Fig. 5 shows the induced peak-to-peak voltage as a function of the pressure difference $P_{\max} - P_{\min}$ in the pressure chamber based on the finite element model. The values of the pressure loads considered are based on the measured pressures in the pressure chamber of a fabricated prototype. The peak-to-peak voltage increases nearly linearly as the pressure difference increases, since the behaviors of the materials are assumed to be linear elastic in the model. For the pressure difference ranging from 21.8 to 41.6 kPa, the maximum and minimum of the generated peak-to-peak voltage are 36.9 and 70.1 mV, respectively. The static analysis for the energy harvester can be used for low frequency applications. The model for estimation of the voltage generated in the piezoelectric film is used for the feasibility study of the proposed energy harvesting device. For more accurate estimation of voltage generation, a dynamic analysis should be carried out.

In the analysis for voltage generation, the pressure within the chamber is assumed to be uniformly distributed. In order to verify this assumption, a three-dimensional flow analysis is carried out using a commercial software FLUENT. In the analysis, a uniform velocity profile at the inlet along the direction of the inlet flow is applied. No-slip (zero velocity) conditions all along the channel walls are specified. The fluid is considered incompressible. It is assumed that only the relative value of pressure is important, and a zero pressure is applied at the outlet of the channel. The Reynolds number is calculated in order to determine if the analysis is in the turbulent region. The Reynolds number of the flow channel can be determined by

$$\mathrm{Re} = \rho U D_h / \mu \tag{5}$$

where U is the flow velocity at the inlet of the diffuser element of the device (see Fig. 2(b)), and μ is the dynamic viscosity of the water, 1.002×10^{-3} Pa $\cdot$ sec . D_h is the hydraulic diameter, which is calculated as 1.5 mm based on the dimension of the rectangular inlet, 2×1.2 mm, of the diffuser element. With the excitation frequency of 45 Hz, the measured maximum value of U based on the experiments is about 118 cm/sec, and the calculated Re is nearly 1766, which can be considered as laminar. Using the laminar model of FLUENT, the pressure distribution of the flow channel is obtained. The deviation of the pressure in the chamber along the symmetry axis is less than 4%, which is quite uniform.

3. Fabrication, experiments and discussions

3.1 Fabrication

In order to verify the effectiveness of the shear mode energy harvester, prototypes of the energy harvester are fabricated. The flow channel is fabricated by carving into a block of acrylic by a milling machine (PNC-3100, Roland DGA Co., Japan). The Ni plate with a diaphragm and a bulge at its center is fabricated by a Ni electroforming process on a stainless steel substrate. Fig. 6 shows the fabrication steps. First, a 10 μm-thick photoresist mould (AZ4260) is coated and patterned over the substrate. Next, a 10 μm-thick Ni layer is electrodeposited using a low-stress nickel sulfamate bath with the chemical compositions listed in Table 2. The bath is kept at a temperature of $45^\circ C$ and a pH value around 4.0. The current density is $1.0\ A/dm^2$. Next, a 50 μm-thick photoresist (JSR THB-126N) is coated and patterned to prepare a mold for electrodeposition of the Ni bulge and Ni plate. Into this mold, a 50 μm-thick Ni layer is electrodeposited using the low-stress nickel sulfamate bath. Following that, the photoresist layer is removed to release the Ni microstructures. Finally, the Ni microstructure is removed from the substrate.

The piezoelectric film is prepared by poling the PZT-5H powder compact that has been sintered and polished. Detail about the fabrication process is described by Cheng et al. [33]. Fig. 7 shows the assembly steps of the energy harvester. First, two glass tubes are glued to the inlet and outlet of the carved flow channel, respectively, by an epoxy adhesive (3M, DP-460), which is cured at a temperature of 45 $^{\circ}$C for 12 hours. Subsequently, the electroformed Ni plate is glued to the flow channel by a thin layer of the epoxy adhesive. Then, the piezoelectric film is glued to the Ni plate and the Ni bulge by applying the epoxy adhesive to complete the assembly steps. The thickness of the adhesive after the assembly step is nearly 30 μm. Finally, two copper wires are welded to the top surface of the piezoelectric film and the Ni plate, respectively, for voltage measurement. Fig. 8(a) and (b) are photos of a fabricated acrylic flow channel and an assembled energy harvester, respectively.

3.2 Experiments

Fig. 9 is a schematic of the experimental apparatus for testing of the fabricated device. The energy harvester is placed on the platform of a tank. In order to provide a pressurized water flow in the pressure chamber of the energy harvester, tap water is pumped into the inlet of the energy harvester through a pulse pump. The oscillating deflection of the piezoelectric film due to the periodic water pressure is measured by a fiberoptic displacement sensor (MTI-2000, MTI Instruments Inc., US). The generated voltage of the piezoelectric film is recorded and analyzed by a data acquisition unit (PCI-5114, National Instruments Co., US). The pressure in the pressure chamber is measured with a subminiature pressure sensor (PS-05KC, Kyowa Electronic Instruments Co. Ltd., Japan) embedded in the pressure chamber. The pressure sensor is connected to a data acquisition unit (DBU-120A, Kyowa Electronic Instruments Co. Ltd., Japan). Fig. 10 is a photo of a close-up view of the experimental apparatus.

The experimental results are shown in Fig. 11. Fig. 11(a) shows the pressure history in the pressure chamber, where the pressure oscillates between 20.8 and -20.8 kPa with a frequency of 45 Hz. The measured deflection history of the center of the piezoelectric film is shown in Fig. 11(b). The film oscillates with an amplitude about 3 $\mu\mathrm{m}$. The measured open circuit voltage generated by the piezoelectric film is shown in Fig. 11(c). The output peak-to-peak voltage for an oscillation amplitude of 20.8 kPa and an excitation frequency of 45 Hz of the pressure in the pressure chamber is nearly 72 $\mathrm{mV_{pp}}$. The experimental results do not show transient responses since they are recorded at steady state vibration. The open circuit voltage as a function of the pressure difference in the pressure chamber ranging from 21.8 to 41.6 kPa is shown in Fig. 5. The experiments are repeated three times and a good repeatability is shown in the figure. The output voltage has a nearly linear relationship to the pressure difference and is in good agreement with the result based on the finite element model except that the slope of the linear regression of the experiments is slightly larger than the finite element analyses. This discrepancy can be attributed to the uncertainties of the material properties, device dimensions, assembly tolerances/alignment, and boundary conditions selected in finite element analyses. The experimental values in Fig. 5 demonstrate that the finite element model provides a relatively accurate prediction of the generated voltage. This indicates that the model can be effective as a design tool to determine the size and excitation pressure level necessary to provide the desired voltage output as far as the behavior of the materials of the device is linear elastic.

In order to evaluate the harvesting system, experiments on the electrical power output of the device are performed. A matched load can be connected to the device to maximize output power. The internal electrical resistance of the device is measured by a LCR meter (WK 4235, Wayne Kerr Electronics, Ltd., UK). The impedance of the probe is 200 $\mathrm{k\Omega}$. The measurement range of the LCR meter is from 0 $\mathrm{M\Omega}$ to 100 $\mathrm{M\Omega}$ at a specified error of less than 1 % over the frequency band 10 Hz – 1 MHz. The instantaneous power can be expressed as

$$P = \frac{(\sqrt{2}\tilde{V})^2}{R} \tag{6}$$

where R is the resistance value of the matched load and $\tilde{V}$ is the root-mean-square value of the voltage drop across the matched load. By connecting the matched load of 1.6 $\mathrm{M\Omega}$ to the device and detecting the voltage drop across the matched load, 0.019 V_{rms}, the instantaneous power is determined as 0.45 nW under an excitation frequency of 45 Hz and a pressure amplitude of 20.8 kPa in the pressure chamber. The power density of the device is estimated as 0.087 $\mu\mathrm{W\ cm^{-3}}$, considering the sum of the volume of the diaphragm, the bulge and the piezoelectric film, 5.15 $\mathrm{mm^3}$.

Fig. 12 shows the vibration amplitude of the center of the piezoelectric film as a function of the excitation frequency based on the experiments. The experiments are repeated three times and the results show a good repeatability of the experiments. The vibration amplitude has a maximum at 45 Hz, which is the excitation frequency used throughout the investigation. The first symmetric resonance frequency of the device based on a finite element analysis is 9042 Hz, where water in the flow channel is not modeled. The first symmetric resonance frequency of the circular diaphragm clamped at its circumference is given as [35]

$$\omega_f = 1.015^2 \frac{\pi^2}{a^2} \sqrt{\frac{Eh^3}{12(1-\nu^2)\rho}} \tag{7}$$

where a and h are the radius and thickness of the circular diaphragm, respectively. E, ν, and ρ are the Young's modulus, Poisson's ratio and density of the material of the diaphragm, respectively. Using Equation (7), the first symmetric resonance frequency of the diaphragm is calculated as 81 Hz. It is expected that the thin diaphragm is relatively flexible compared to the structure of the bulge and the piezoelectric film, and the diaphragm behaves similarly to a diaphragm loaded at its center and constrained at its circumference. Therefore, the energy harvester has a peak vibration amplitude at 45 Hz, which is near the calculated resonance frequency, 81 Hz, of the circular diaphragm. Furthermore, resonant frequencies are expected to decrease in a water environment, since water affects the viscous damping of the structure and adds hydromass to it [36,37].

In this investigation, the device is operated at a specific frequency, 45 Hz. Most energy harvesting device based on piezoelectric effects have focused on single-frequency ambient energy, i.e. resonance-based energy harvesting [38]. When the ambient excitation is at a single frequency, the design of the energy harvesting device can be tailored to the ambient frequency available. For random and broadband ambient flow sources, the device may not be robust. To account for the variations in the excitation frequency, a device with an array of structures with various resonance frequencies can be utilized [23]. The other possible route to account for the random ambient flow sources is to minimize the mechanical damping or maximize the electromechanical coupling of the device [38]. A structure with multiple resonant frequencies may also be considered for energy harvesting from random vibrations with multiple resonant peaks, for example a segmented composite beam with embedded piezoelectric layers [26]. As shown in Fig. 12, the device is sensitive to frequency drift, it is not applicable where a single frequency ambient energy source is not available. In order to account for the frequency drift in the ambient energy source, new designs of the device must be investigated for its potential applications in power supply of remote wireless sensors.

In order to generate the pressure fluctuation in the channel, a pulse pump is used to pump tap water into the flow channel in the laboratory environment. Energy can be harvested from unsteady geophysical flows (ocean or river currents) or random fluctuation of tire pressure due to ambient temperature changes or contact between vehicle tire and pavement surface. The power output at $0.45\ \mathrm{nW}$ of the presented device is quite low so as the measurement errors caused by parasite effects may be in the same order. The measured capacitance of the device is nearly 93 pF, which may include the contributions from the piezoelectric film and the parasitic effects. The piezoelectric film is $3\,\mathrm{mm}\times 4\,\mathrm{mm}$ by 0.2 mm thick and its capacitance is estimated as 47 pF based on the capacitance of the piezoelectric material, PZT-5H, 389 $\mathrm{pF}\cdot\mathrm{cm}^{-2}$ (see Table 1). The parasitic capacitance of the experimental setup is estimated as 46 pF. The power output of the device should be improved for better accuracy of the test results.

Compared to the power density of the 31 mode piezoelectric cantilever of Fang et al. [6], 10843 $\mu\mathrm{W\ cm}^{-3}$, and the 15 mode piezoelectric cantilever of Ren et al. [17], 24762 $\mu\mathrm{W\ cm}^{-3}$, the power density of the presented device, 0.087 $\mu\mathrm{W\ cm}^{-3}$, is too low. The power density of the device should be increased for at least two orders to prove its feasibility. In order to obtain a higher output power of the shear mode piezoelectric energy harvester, the dimensions and structure of the device can be optimized, and a piezoelectric material with higher piezoelectric constants can be adopted. It is possible to increase the power density by one order of magnitude by replacing the piezoelectric material, PZT-5H, which has a d_{15} value of 741 $\mathrm{pm \cdot V^{-1}}$, with the single crystal of PMN-0.29PT ($0.71Pb(Mg_{1/3}Nb_{2/3})O_3 - 0.29PbTiO_3$) as the piezoelectric material due to its ultrahigh d_{15} value of 5980 $\mathrm{pm \cdot V^{-1}}$ [17]. Given that the values of the capacitance and stiffness of PZT-5H and PMN-0.29PT are of the same order and the d_{15} value of PMN-0.29PT is nearly ten times larger than that of PZT-5H, the power density of the presented device with PMN-0.29PT as the material of the piezoelectric film can be increased by one order.

The experimental results of Fig. 5 reveal that the open circuit voltage has a nearly linear relationship for the pressure difference in the pressure chamber ranging from 21.8 to 41.6 kPa. The slope of the linear regression of the experiments is nearly 2 mV/kPa. Based on Eq. (6), a ten fold increase in the power can be accomplished by increasing the pressure difference in the pressure chamber by approximately three times as far as the behavior of the materials of the device remains linear elastic. Edery-Azulay and Abramovich [16] pointed out that by decreasing the length or width of the 15 mode piezoelectric beam and increasing its thickness while keeping its volume the same, the efficiency of the 15 mode can become much larger. This fact could be considered as an alternative for increasing the power density of the presented device.

Finite element analyses of the device with a piezoelectric film with a d_{15} value of 7410 $\mathrm{pm \cdot V^{-1}}$ are carried out. Keeping all other material properties of the piezoelectric film the same as the PZT-5H and under a pressure difference $P_{\max} - P_{\min}$ in the pressure chamber of 400 kPa, the generated peak-to-peak voltage is 5614.5 mV. Assuming a matched load of 1.6 $\mathrm{M\Omega}$ to the device as the experiments and a voltage drop across the matched load, 5614.5 $\mathrm{mV_{pp}}$, the instantaneous power is determined as 4.9 $\mu\mathrm{W}$. The output power of the proposed improved design has a four-order increase compared to the experimental device, 0.45 nW.

4. Conclusions

A shear mode piezoelectric energy harvester is developed. The energy is harvested from a pressurized water flow. The pressure oscillation in the pressure chamber of the harvester results in a periodical deflection of the piezoelectric film and therefore the voltage generation. A finite element model of the output voltage of the device is developed for quick evaluation of the effects of device dimensions, pressure loads and material properties on the performance of the energy harvester. Prototypes of the energy harvester are fabricated and tested. The measurements conducted in various pressure difference in the pressure chamber of the device show that the maximum generated voltage and instantaneous power are approximately 72 $\mathrm{mV_{pp}}$ and 0.45 nW, respectively, when the excitation pressure oscillates with an amplitude of 20.8 kPa and a frequency of about 45 Hz. The generated voltages based on the finite element model agree well with the experiments. The model can be used to predict the performance of the energy harvester with different dimensions, material properties and pressure loads.

Sources of pressurized water flow can be throttling valves of water pipelines and throttles in automotive applications, or unsteady geophysical flows. The periodic vortex shedding behind a blunt body immersed in a steady stream causes a pressure oscillation in the stream. This regular, periodic shedding can be integrated into the flow channel of the proposed device to scavenge the flow energy.

Acknowledgement

This work is financially supported by a grant from National Science Council, Taiwan (Grant Number: NSC 99-2221-E-005-075). Partial support of this work by Precision Machinery Research and Development Center (Contract Number: 98TR10) is greatly appreciated. The authors would like to express their appreciation to the National Center for High-Performance Computing (NCHC), Taiwan for their assistance. Helpful discussions with Professor Yung Ting of Chung Yuan Christian University, Taiwan, R.O.C. are greatly appreciated.

References

[1] Z. Wang, V. Leonov, P. Fiorini, C. Van Hoof, Realization of a wearable miniaturized thermoelectric generator for human body applications, Sensors and Actuators A 156 (2009) 95-102.

[2] D. Krähenbühl, C. Zwyssig, H. Weser, J.W. Kolar, Theoretical and experimental results of a mesoscale electric power generation system from pressurized gas flow, Journal of Micromechanics and Microengineering 19 (2009) 094009.

[3] J. J. Allen and A. J. Smits, Energy harvesting eel, Journal of Fluid and Structures, 15 (2001) 629-640.

[4] T. Starner, Human-powered wearable computing, IBM Systems Journal, 35 (1996) 618-629.

[5] N. M. White, P. Glynne-Jones and S. P. Beeby, A novel thick-film piezoelectric micro-generator, Smart Materials and Structures, 10 (2001) 850-852.

[6] H.-B. Fang, J.-Q. Liu, Z.-Y. Xu, L. Dong, L. Wang, D. Chen, B.-C. Cai, Y. Liu, Fabrication and performance of MEMS-based piezoelectric power generator for vibration energy harvesting, Microelectronics Journal, 37 (2006) 1280-1284.

[7] F. Lu, H. P. Lee and S. P. Lim, Modeling and analysis of micro piezoelectric power generators for micro-electromechanical-systems applications, Smart Materials and Structures, 13 (2004) 57-63.

[8] R. Guigon, J.-J. Chaillout, T. Jager and G. Despesse, Harvesting raindrop energy: experimental study, Smart Materials and Structures, 17 (2008) 015039.

[9] Z. L. Wang, Energy harvesting for self-powered nanosystems, Nano Research, 1 (2008) 1-8.

[10] Q. Zheng and Y. Xu, Asymmetric air-spaced cantilevers for vibration energy harvesting, Smart materials and Structures, 17 (2008) 055009.

[11] T. Wacharasindhu and J. W. Kwon, A micromachined energy harvester from a keyboard using combined electromagnetic and piezoelectric conversion, Journal of Micromechanics and Microengineering, 18 (2008) 104016.

[12] B. S. Lee, S. C. Lin, W. J. Wu, X. Y. Wang, P. Z. Chang, C. K. Lee, Piezoelectric MEMS generators fabricated with an aerosol deposition PZT thin film, Journal of Micromechanics and Microengineering, 19 (2009) 065014.

[13] D. Shen, J.-H. Park, J. Ajitsaria, S.-Y. Choe, H.C. Wikle III, D.-J. Kim, The design, fabrication and evaluation of a MEMS PZT cantilever with an integrated Si proof mass for vibration energy harvesting, Journal of Micromechanics and Microengineering 18 (2008) 055017.

[14] M. Marzencki, Y. Ammar, S. Basrour, Integrated power harvesting system including a MEMS generator and a power management circuit, Sensors and Actuators A 145-146 (2008) 363-370.

[15] Y.B. Jeon, R. Sood, J.-H. Jeong, S.-G. Kim, MEMS power generator with transverse mode thin film PZT, Sensors and Actuators A 122 (2005) 16-22.

[16] L. Edery-Azulay, H. Abramovich, Piezoelectric actuation and sensing mechanisms – closed form solutions, Composite Structures 64 (2004) 443-453.

[17] B. Ren, S.-W. Or, Y. Zhang, Q. Zhang, X. Li, J. Jiao, W. Wang, D. Liu, X. Zhao, H. Luo, Piezoelectric energy harvesting using shear mode $0.71Pb(Mg_{1/3}Nb_{2/3})O_3 - 0.29PbTiO_3$ single crystal cantilever, Applied Physics Letters 96 (2010) 083502.

[18] C. Majidi, M. Haataja, D.J. Srolovitz, Analysis and design principles for shear-mode piezoelectric energy harvesting with ZnO nanoribbons, Smart Materials and Structures 19 (2010) 055027.

[19] N.G. Stephen, On energy harvesting from ambient vibration, Journal of Sound and Vibration 293 (2006) 409-425.

[20] S.-N. Chen, G.-J. Wang, M.-C. Chien, Analytical modeling of piezoelectric vibration –induced micro power generator, Mechatronics 16 (2006) 379-387.

[21] A. Erturk, D.J. Inman, Issues in mathematical modeling of piezoelectric energy harvesters, Smart Materials and Structures 17 (2008) 065016.

[22] F. Goldschmidtboeing, P. Woias, Characterization of different beam shapes for piezoelectric energy harvesting, Journal of Micromechanics and Microengineering 18 (2008) 104013.

[23] J.-Q. Liu, H.-B. Fang, Z.-Y. Xu, X.-H. Mao, X.-C. Shen, D. Chen, H. Liao and B.-C. Cai, A MEMS-based piezoelectric power generator array for vibration energy harvesting, Microelectronics Journal, 39 (2008) 802-806.

[24] A. Erturk, D.J. Inman, An experimentally validated bimorph cantilever model for

piezoelectric energy harvesting from base excitations, Smart Materials and Structures 18 (2009) 025009.

[25] M. Marzencki, M. Defosseux, S. Basrour, MEMS vibration energy harvesting devices with passive resonance frequency adaptation capability, Journal of Microelectromechanical Systems 18 (2009) 1444-1453.

[26] S. Lee, B. D. Youn and B. C. Jung, Robust segment-type energy harvester and its application to a wireless sensor, Smart Materials and Structures, 18 (2009) 095021.

[27] C.T. Pan, Z.H. Liu, Y.C. Chen, C.F. Liu, Design and fabrication of flexible piezo-microgenerator by depositing ZnO thin films on PET substrates, Sensors and Actuators A 159 (2010) 96-104.

[28] D. Benasciutti, L. Moro, S. Zelenika, E. Brusa, Vibration energy scavenging via piezoelectric bimorphs of optimized shapes, Microsystem Technologies 16 (2010) 657-668.

[29] G.W. Taylor, J.R. Burns, S.M. Kammann, W.B. Powers, T.R. Welsh, The energy harvesting eel: A small subsurface ocean/river power generator, IEEE Journal of Oceanic Engineering, 26 (2001) 539-547.

[30] L. Tang, M.P. Païdoussis, J. Jiang, Cantilevered flexible plates in axial flow: Energy transfer and the concept of flutter-mill, Journal of Sound and Vibration, 326 (2009) 263-276.

[31] S. Roundy, P.K. Wright, A piezoelectric vibration based generator for wireless electronics, Smart Materials and Structures 13 (2004) 1131-1142.

[32] T. Rödig, A. Schönecker, G. Gerlach, A survey on piezoelectric ceramics for generator applications, Journal of the American Ceramic Society 93 (2010) 901-912.

[33] C.H. Cheng, S.C. Chen, S.W. Young, Y.R. Su, Y.C. Lin, Effect of poling conditions on out-of-plane displacement for a shear mode PZT actuator, Sensors and Actuators A 126 (2006) 386-395.

[34] H. D. Hibbitt, B. I. Karlsson. E. P. Sorensen, *ABAQUS user manual*, Version 6-2, HKS Inc., Providence, RI, USA, 2001.

[35] L. Meirovitch, Principles and techniques of vibrations, Prentice-Hall Inc., Upper Saddle River, New Jersey, USA, 1997.

[36] N. Piccirillo, Analysis of fluid-structural instability in water, Proc. SPIE Vol. 3089,

Proceedings of the 15th International Modal Analysis Conference, pp. 343-349, 1997.

[37] R. J. Fritz, The effect of liquids on the dynamic motions of immersed solids, Transactions of ASME, Journal of Engineers for Industry 94 (1972) 167-173.

[38] S. Adhikari, M.I. Friswell, D.J. Inman, Piezoelectric energy harvesting from broadband random vibrations, Smart Materials and Structures 18 (2009) 115005.

Biography

Dung-An Wang received the Ph.D. degree in mechanical engineering from the University of Michigan at Ann Arbor, in 2004. He is currently an Associate Professor in the Graduate Institute of Precision Engineering, National Chung Hsing University, Taiwan, ROC. His research interests include micromachined resonators and actuators, piezoelectric actuators, microassembly and compliant mechanisms.

Nine-Zeng Liu received the M.S. degree in the Graduate Institute of Precision Engineering, National Chung Hsing University, Taiwan, ROC, in 2010. His research interests are piezoelectric actuators, and energy harvesters.

List of figures

Table 1. Properties of the piezoelectric film (PZT-5H), the electrodes (silver) and the bulge and the diaphragm (Ni)

	Property	Tensor (in order of *x*, *y*, *z*, *xy*, *xz*, *yz*)
PZT-5H	Piezoelectricity **d** ($m \cdot V^{-1}$)	$10^{-12} \times \begin{bmatrix} 0 & 0 & 0 & 741 & 0 & 0 \\ -274 & 593 & -274 & 0 & 0 & 0 \\ 0 & 0 & 0 & 0 & 0 & 741 \end{bmatrix}$
	Permittivity ε ($F \cdot m^{-1}$)	$10^{-9} \times \begin{bmatrix} 15.052 & 0 & 0 \\ 0 & 13.015 & 0 \\ 0 & 0 & 15.052 \end{bmatrix}$
	Density ($kg \cdot m^{-3}$)	7600
	Stiffness C (N m^{-2})	$10^{10} \times \begin{bmatrix} 12.60 & 8.41 & 7.95 & 0 & 0 & 0 \\ & 11.70 & 8.41 & 0 & 0 & 0 \\ & & 12.60 & 0 & 0 & 0 \\ & & & 2.30 & 0 & 0 \\ & \text{symmetric} & & & 2.30 & 0 \\ & & & & & 2.30 \end{bmatrix}$
	Capacitance ($pF \cdot cm^{-2}$	389
Silver	Density ($kg \cdot m^{-3}$)	10500
	Young's modulus (GPa)	83
	Poisson's ratio	0.37
Ni	Density ($kg \cdot m^{-3}$)	7780
	Young's modulus (GPa)	210
	Poisson's ratio	0.3

Table 2. Chemical compositions of the low-stress nickel electroplating solution

Chemical	Amount (g/L)
Nickel sulfamate, $Ni(NH_2SO_3)_2 \cdot 4H_2O$	300
Nickel chloride, $NiCl_2 \cdot 6H_2O$	4
Boric acid, H_3BO_3	40
Wetting agent	3
Deionized water	to 1 L

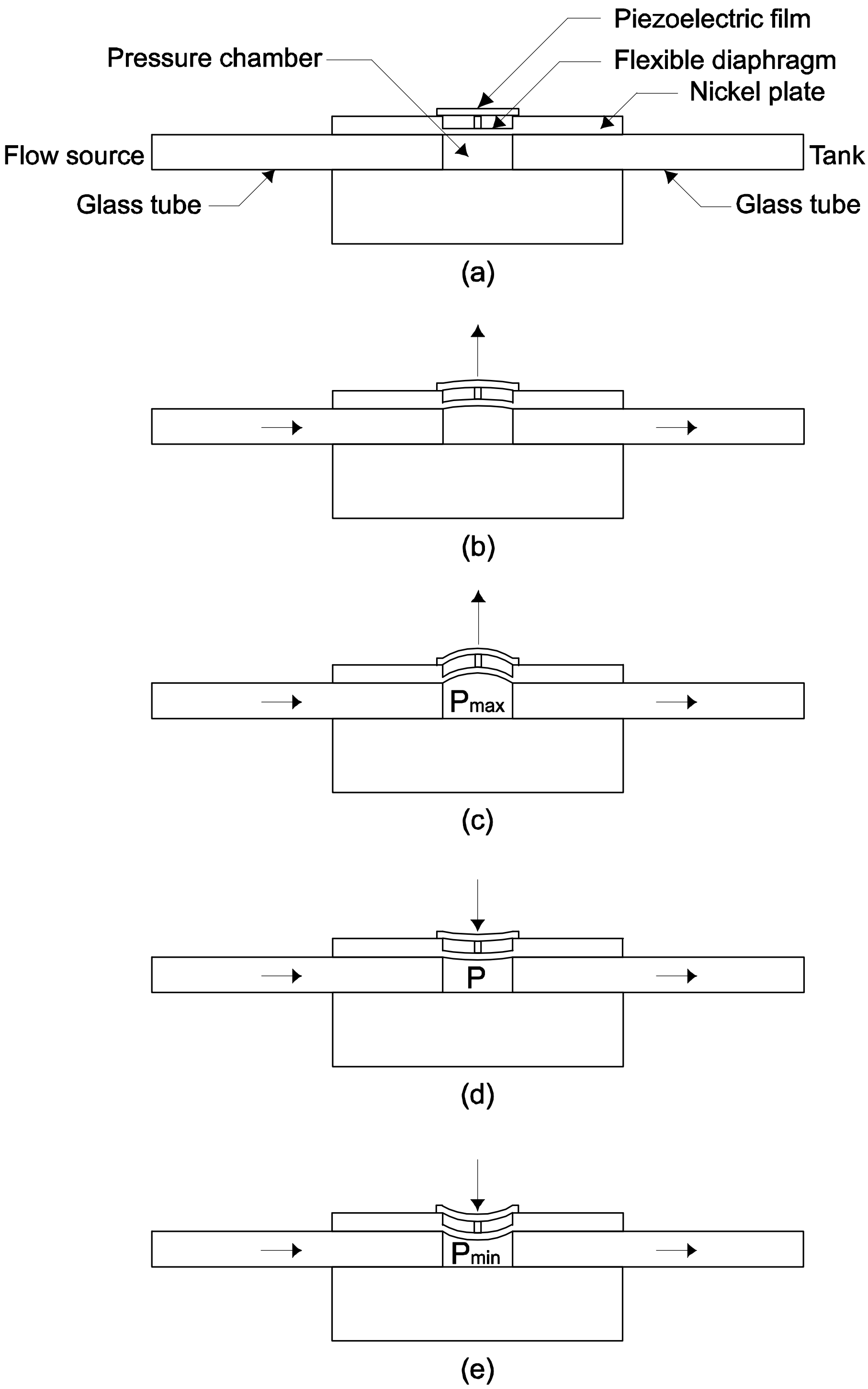

Fig. 1. Operation of a piezoelectric energy harvester.

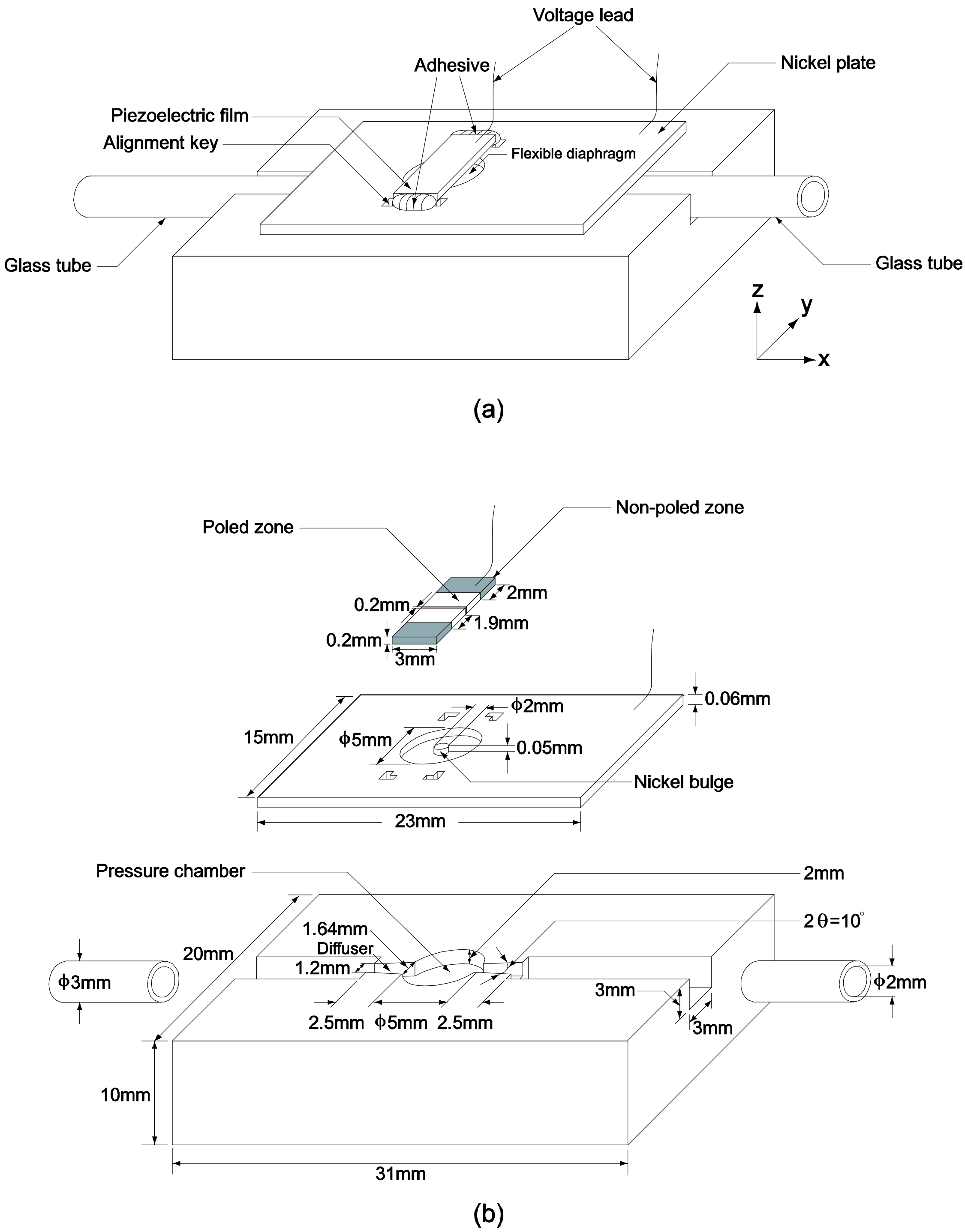

Fig. 2. (a) An assembled energy harvester. (b) Components of the energy harvester.

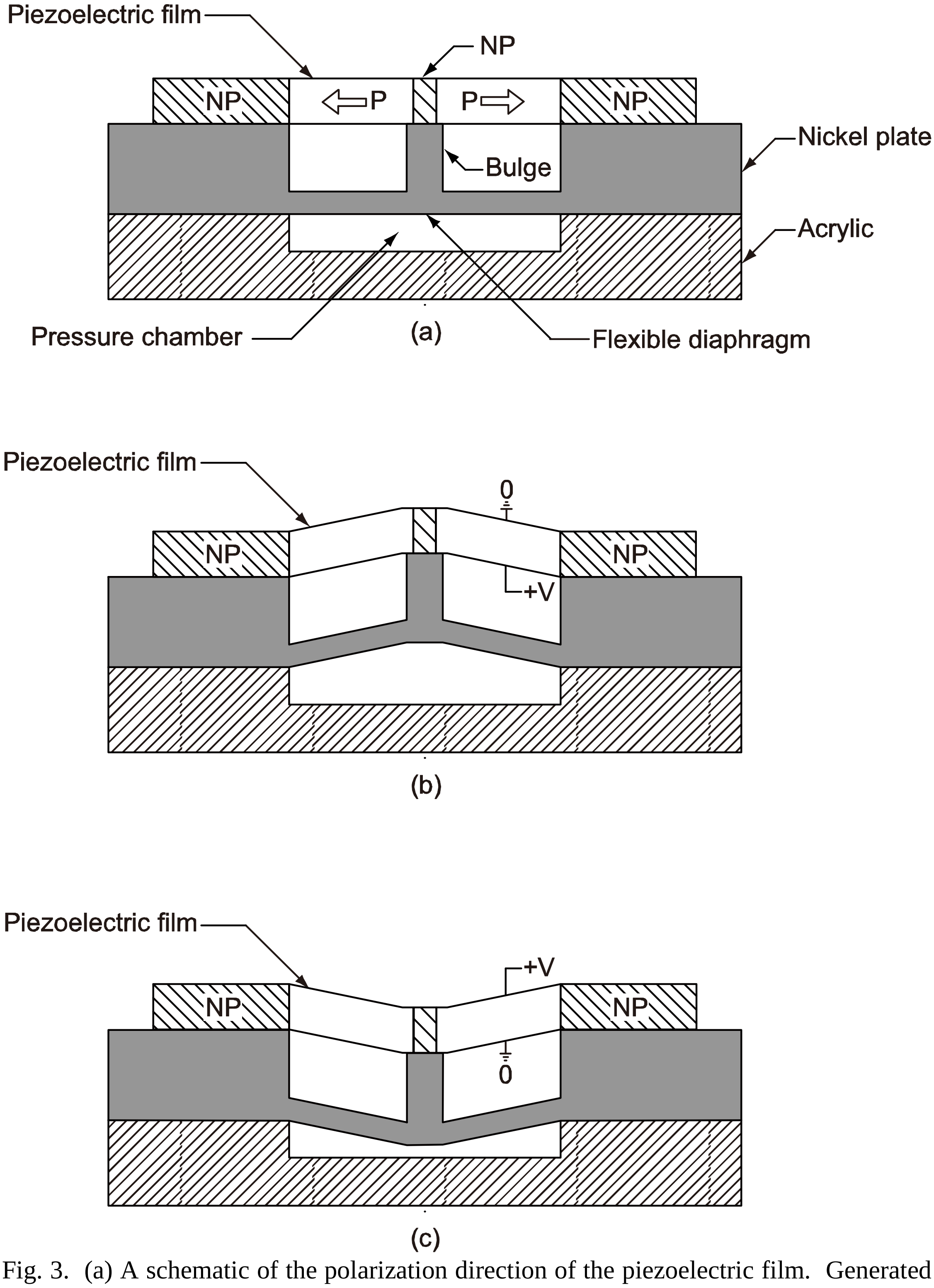

Fig. 3. (a) A schematic of the polarization direction of the piezoelectric film. Generated electrical field in the piezoelectric film when the Ni diaphragm move upward (b), or downward (c).

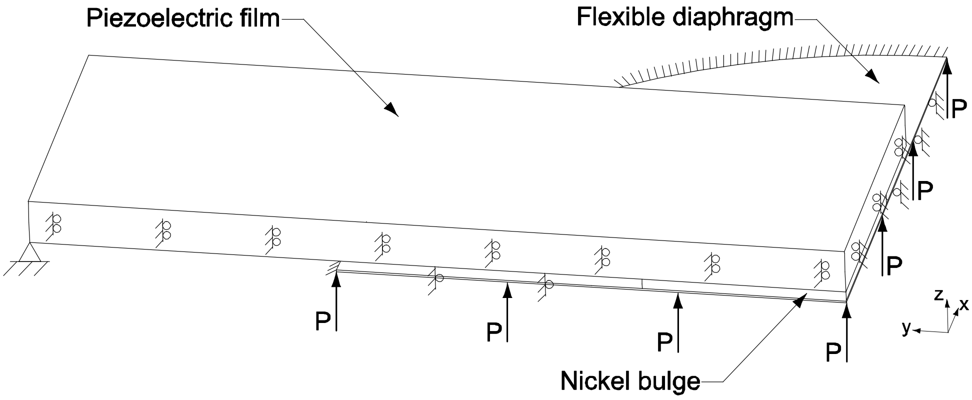

(a)

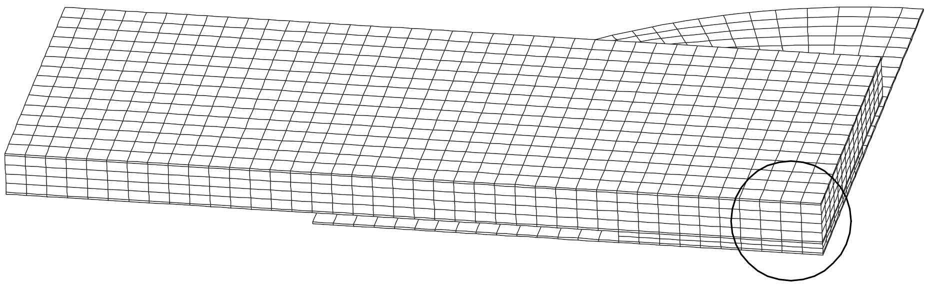

(b)

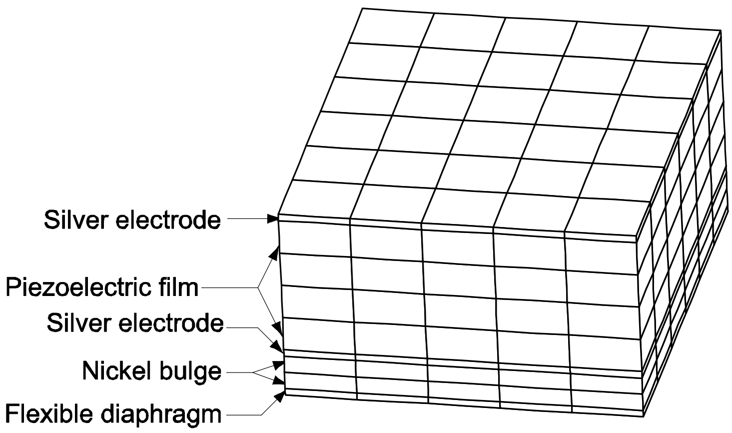

(c)

Fig. 4. (a) A schematic of a quarter model of the piezoelectric film, bulge and flexible diaphragm. (b) A finite element mesh of the quarter model. (c) A close-up view of the mesh near the center of the diaphragm.

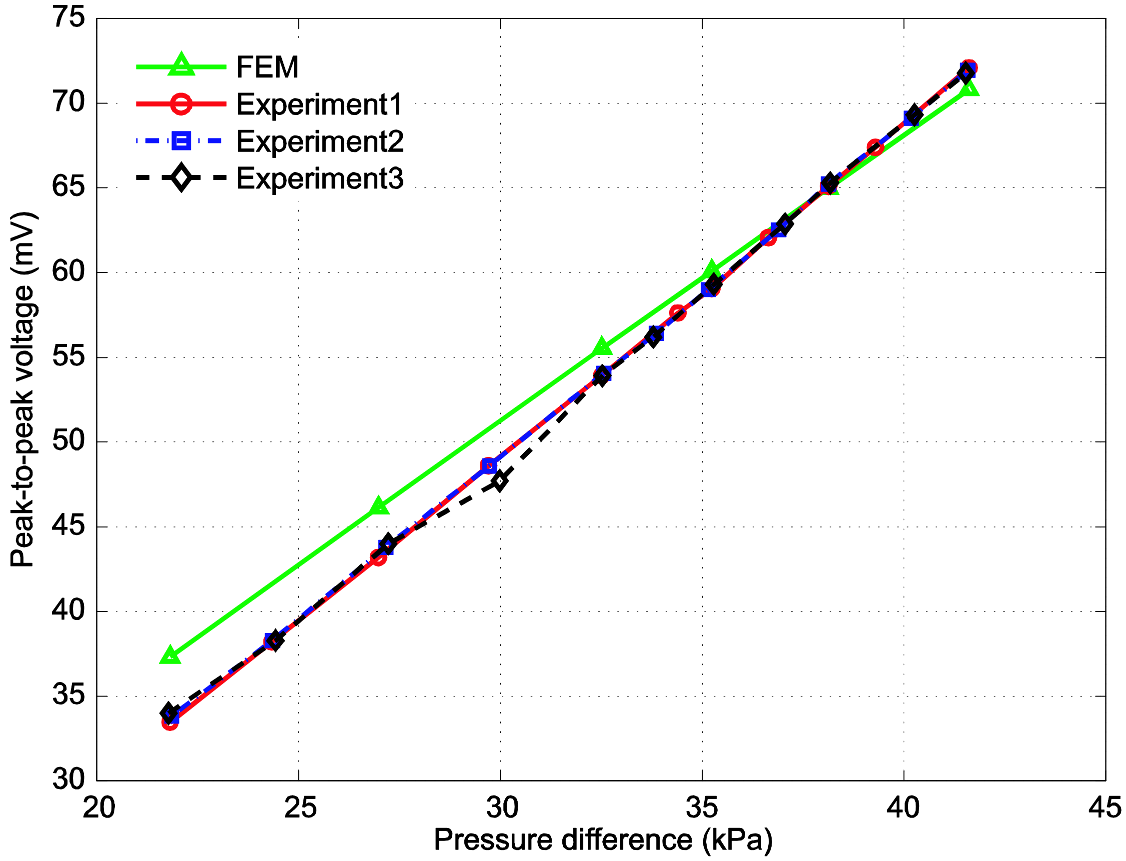

Fig. 5. Generated peak-to-peak voltage as a function of the pressure difference in the pressure chamber.

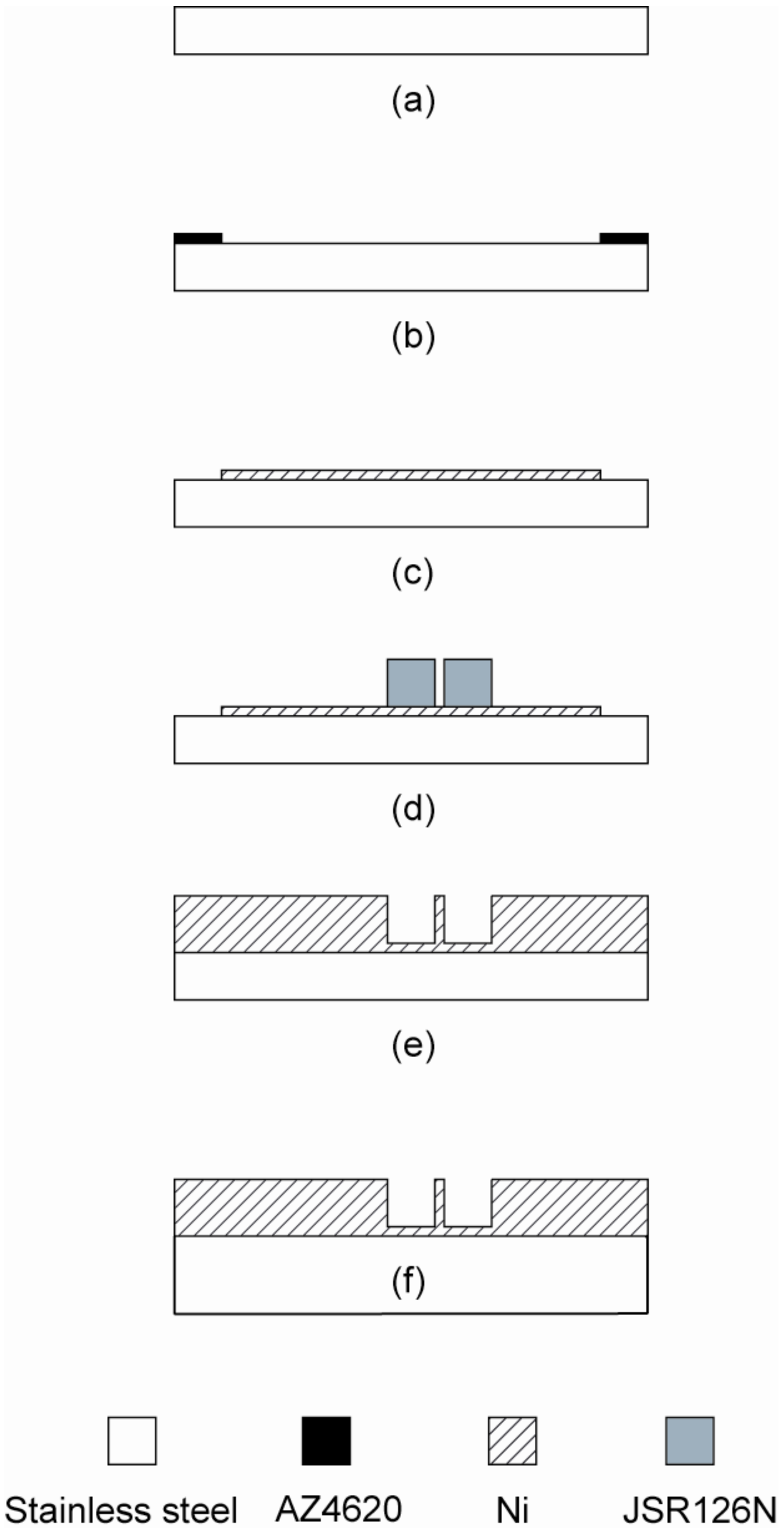

Fig. 6. Fabrication steps of the nickel diaphragm.

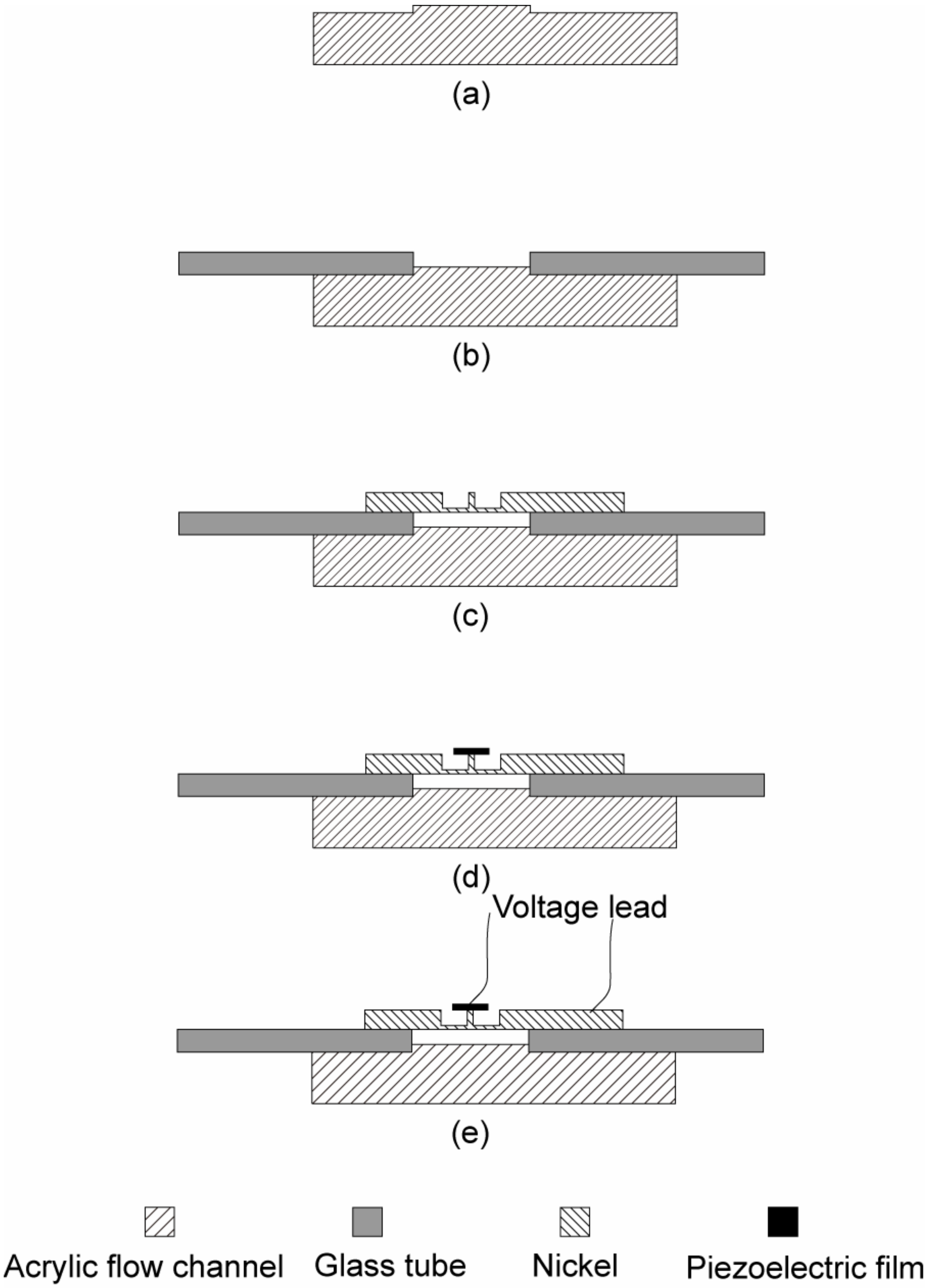

Fig. 7. Assembly steps of the energy harvester.

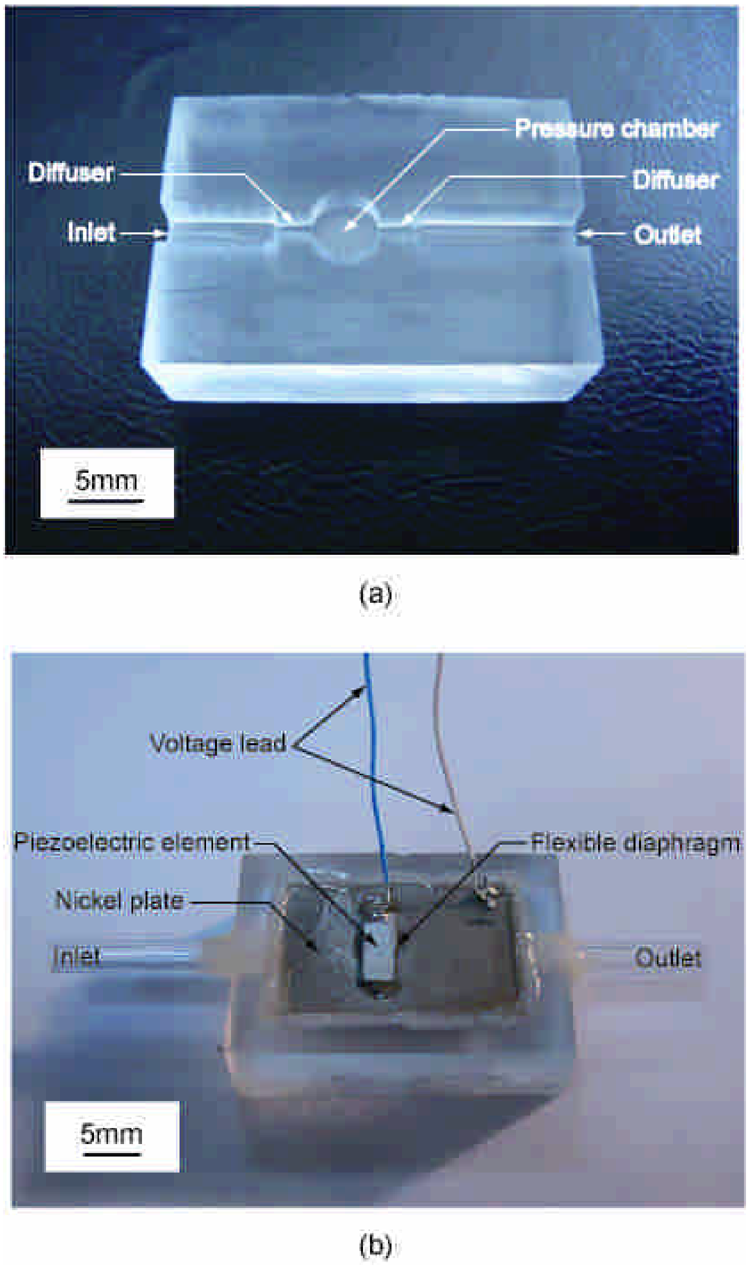

Fig. 8. (a) Fabricated acrylic channel. (b) Assembled energy harvester.

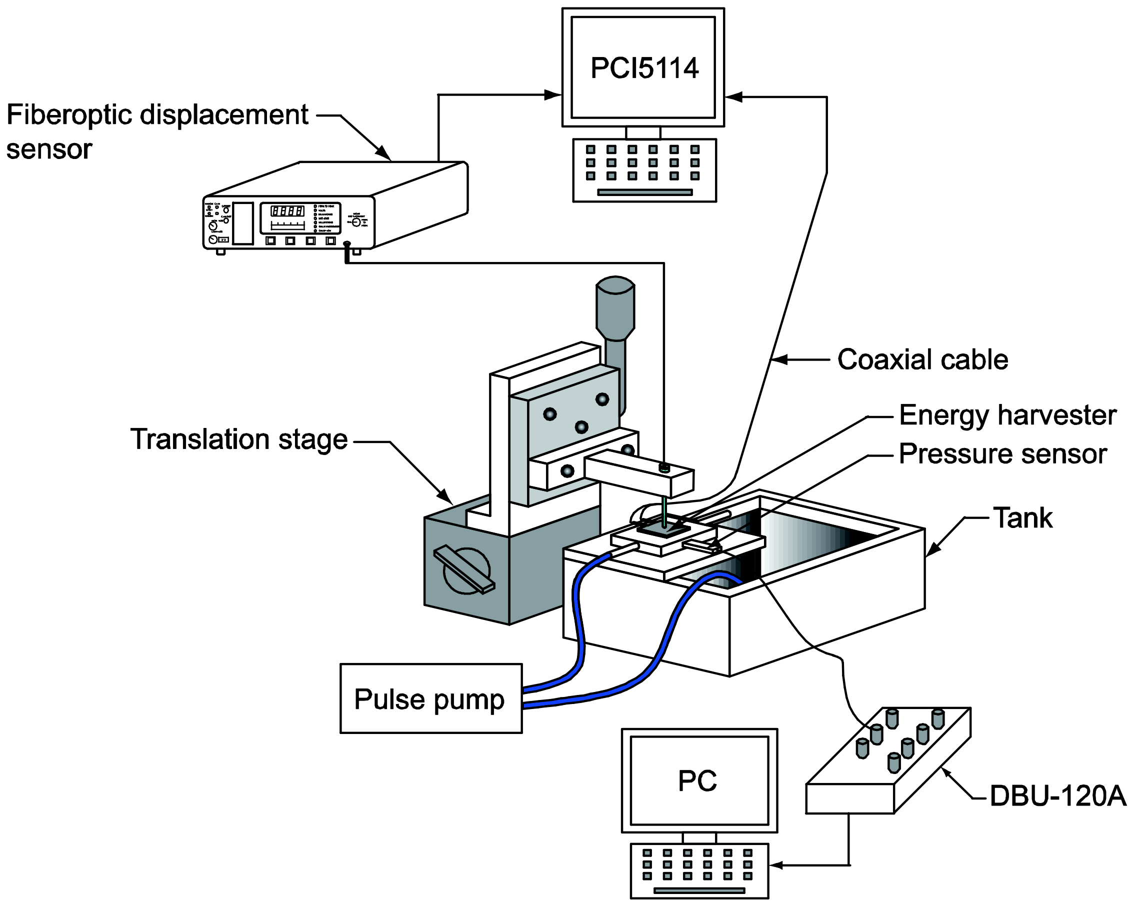

Fig. 9. Schematic of the experimental apparatus.

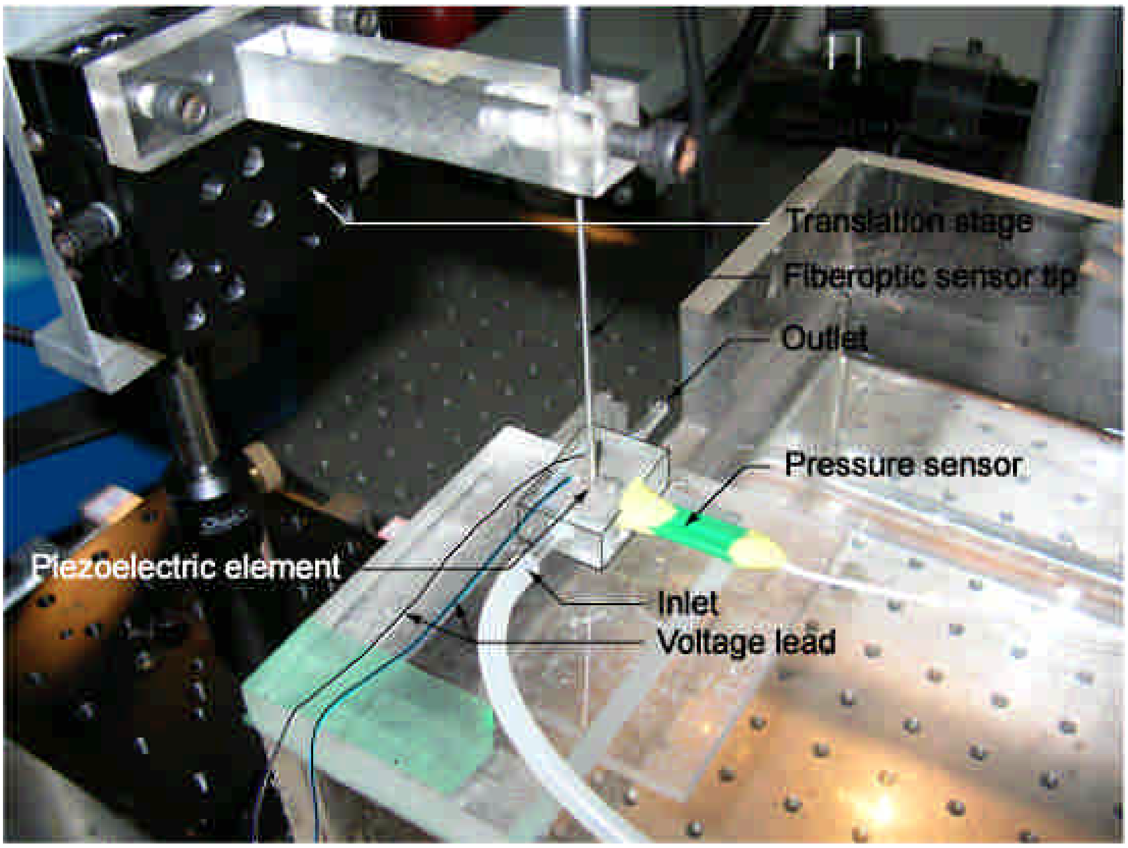

Fig. 10. Close-up view of the experimental apparatus.

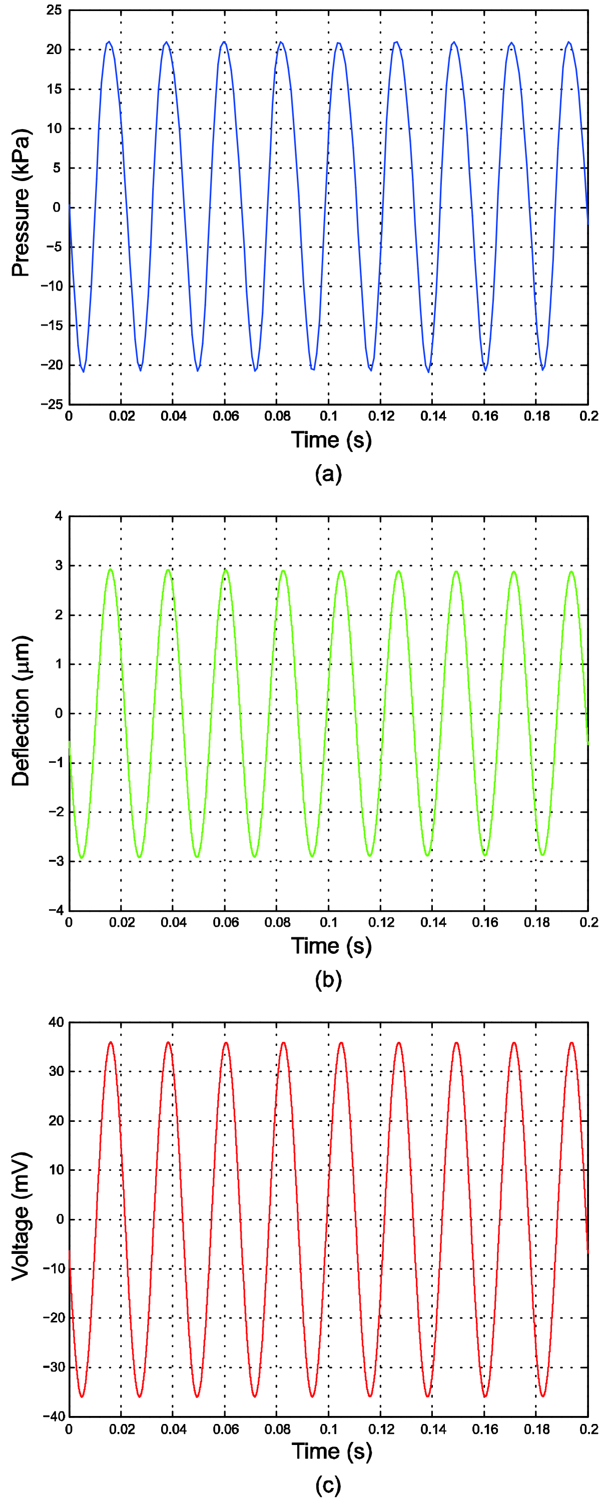

Fig. 11. Experimental results. (a) Pressure variation in the pressure chamber. (b) Deflection of the center of the piezoelectric film. (c) Output voltage of the piezoelectric film.

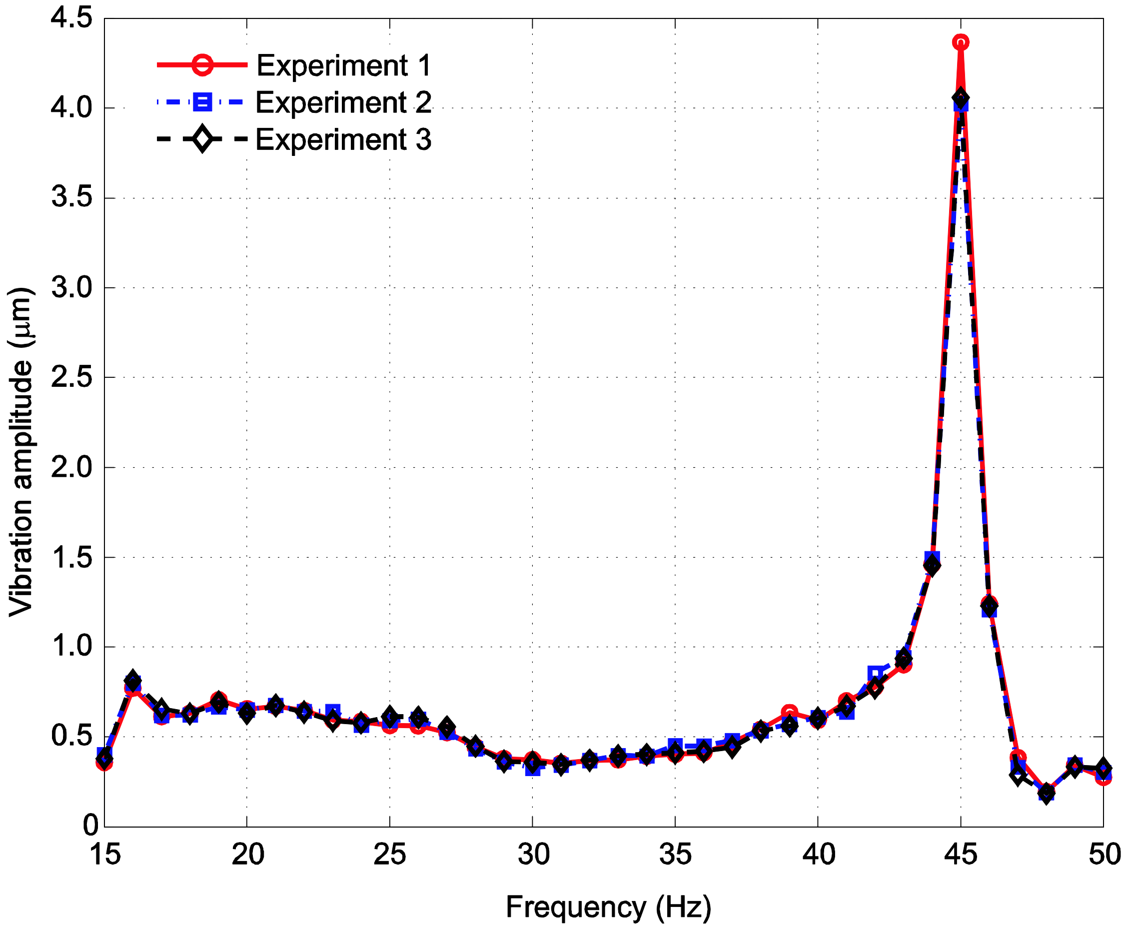

Fig. 12. The vibration amplitude of the center of the piezoelectric film as a function of the excitation frequency based on the experiments.